# Influence of Mechanical Properties of Agarose Hydrogels on Bacterial Growth and Secretory Activity

L. Dupont[a], V. S. Tadimarri[b], R. Buret[c], S. Sankaran[b], L. Picton[c], A. M. Jonas[*,a,d], K. Glinel[*,a]

[a] Institute of Condensed Matter and Nanosciences, Bio and Soft Matter, Université catholique de Louvain (UCLouvain), Louvain-la-Neuve, Belgium

[b] Leibniz Institute for New Materials, Universität des Saarland, Saarbrücken, Germany

[c] Laboratoire Polymères, Biopolymères, Surfaces, Université de Rouen, France

[d] WEL Research Institute, Avenue Pasteur 6, 1300 Wavre, Belgium

*Corresponding authors: karine.glinel@uclouvain.be; alain.jonas@uclouvain.be

**ABSTRACT**

Engineered living materials (ELMs) rely on the ability to control cell behavior in material systems. ELMs containing bacteria secreting beneficial molecules are being developed for therapeutic purposes. Using commensal strains embedded in physically cross-linked agarose hydrogels, we systematically investigate how gel rigidity and initial bacterial density affect the morphology of bacterial colonies and their secretory function. Although often considered independently, these parameters jointly define the microscale environment experienced by embedded cells, influencing nutrient access, mechanical interactions, and potential cell-to-cell communication. We show that matrix rigidity effectively tunes aggregate morphology, modulating their shape and compactness, without compromising bacterial growth or secretion. In parallel, initial bacterial density determines the biomass accumulation dynamics and spatial distribution of aggregates, which in turn influence the onset and temporal profile of secretory activity, without altering its final magnitude. This decoupling between structural organization

and secretory output opens new possibilities for engineering ELMs with tailored architectures and prolonged secretory and release activity.

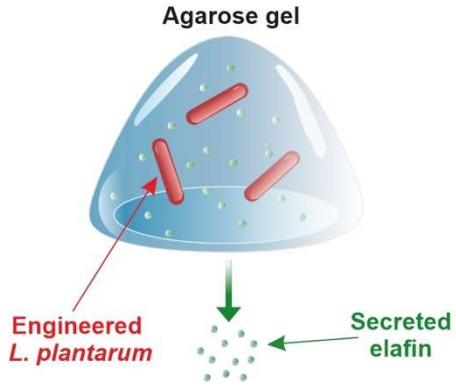


## Introduction

Commensal bacteria, which are closely associated with human health and contribute to protection against certain diseases, are increasingly recognized as promising candidates for living therapeutics [1]. However, the use of living bacteria in biomedical applications requires overcoming some essential challenges while respecting regulatory requirements, notably maintaining bacterial viability and activity to ensure their therapeutic effect, as well as eliminating potentially adverse effects of commensal bacteria turning opportunistic if left free to proliferate [2–4]. It is therefore important to develop safe and effective strategies that enable the clinical applicability of bacteria-based therapies. Among these, the encapsulation of bacterial cells in a polymer matrix allowing diffusion of nutrients and secreted molecules while still prolonging cellular viability and activity but limiting cell dissemination, has emerged as a promising approach. Such materials comprising active micro-organisms belong to the class of engineered living materials (ELMs) [5,6]. Here, we investigate the inclusion of commensal bacterial in gelled media of different mechanical strengths and study the morphology of growing bacterial colonies and its impact on their secretory activity, aiming at finding conditions for prolonged and slow release of a model therapeutic protein.

Materials used in ELMs mainly include hydrogels which mimic the natural biofilm environment. Thanks to their 3D structure, high water content, biocompatibility, and tunable

physicochemical and viscoelastic properties [1,7,8], they can protect bacterial cells from environmental assaults [9,10]. Hydrogels can be either natural or synthetic and are classified as physical or chemical depending on the type of cross-linking involved in the formation of their macromolecular network [11]. The natural polymers most frequently used for cell encapsulation are agarose [12–16], gelatin [17,18], carrageenan [19,20], dextran [21], or alginate [4,22]; among synthetic polymers, polyvinyl alcohol [23,24], polyacrylamide [25] or Pluronic [26–30], chemically modified or not [31], are frequent choices. The selection of the hydrogel in which bacterial cells are incorporated is crucial for the development of ELMs because it provides the environmental cues that govern cell fate. For instance, bacteria encapsulated in covalently cross-linked polyacrylamide hydrogels often show reduced viability and metabolic activity, in contrast to those embedded in physically cross-linked hydrogels like agarose [13]. Other works have shown that increasing matrix rigidity can lead to changes in gene expression [32], reduced growth kinetics [14], formation of compact cellular aggregates [17,18], higher resistance to diverse antibiotics [15], as well as different secretion profiles depending on the degree of mechanical stress exerted on cells [29]. However, the conclusions from literature may differ or are incomplete depending on the nature of the polymer matrix and the protocols used. It is therefore important to improve our current understanding of bacterial behavior in different hydrogel matrices and to elucidate the conditions under which mechanical constraints have a significant impact on their physiology, including growth kinetics, morphodynamics, spatial distribution, and most importantly secretory activity. This would help us develop rational design guidelines for ELMs encapsulating bacteria for therapeutic applications.

In this context, the objective of this work is to identify how the rheological properties of physically cross-linked nutrient-containing hydrogels embedding commensal bacteria may control their proliferation and activity, in the absence of an external nutrient source. Agarose, a

heteropolysaccharide obtained after purification of agar extracted from red algae, was selected as the embedding matrix. The macromolecular chains consist of repeating units of D-galactose and 3,6-anhydro-L-galactose linked by α- and β-glycosidic bonds. Agarose forms a thermoreversible physical hydrogel *via* chain aggregation upon cooling [33,34], allowing to easily incorporate bacteria in mild non-detrimental conditions. Unlike chemically cross-linked gels, these hydrogels possess a dynamic microstructure that can rearrange under the forces exerted by growing cells, potentially allowing them to expand in parallel to the kinetics of gel reorganization. The biocompatible properties, structural stability, high water content and microbial inertness make agarose gels particularly suitable for studying growth dynamics of encapsulated bacteria [33,35–37]. Importantly, their rheological properties are affected not only by the polymer concentration [38] but also by the algal sources and extraction methods [33,36], content and degree of regularity of alternation of D-galactose and 3,6-anhydro-L-galactose residues [39,40], molar mass [41,42] and degree of desulfation of its native polysaccharide agar [43] (determining the proportion of anhydrous units in the agarose backbone). These factors affect how agarose chains self-assemble and align into a macromolecular network during gel formation [44–46], leading to varying degrees of crystallinity and giving rise to distinct commercial grades of agarose. In particular, highly crystalline agaroses form well-ordered double helices that interact to create strong, rigid gel networks with high melting points. In contrast, amorphous agaroses exhibit more irregular chain packing, resulting in softer, weaker gels. Therefore, the suitability of agarose hydrogels for practical applications can be tuned by two main parameters: the gel strength and the hysteresis between the gelling and the melting temperatures [35].

In this study, agarose hydrogels having different rheological properties, obtained by varying the agarose concentration or grade, were used to embed two beneficial, gram-positive and non-

96 motile commensal bacterial strains, namely *Staphylococcus epidermidis* (*S. epidermidis*) and
97 *Lactiplantibacillus plantarum* (*L. plantarum*), differing by their shape (sphere *versus* rod,
98 respectively). We systematically investigate how the rheological characteristics of the
99 surrounding matrix influence bacterial proliferation, morphodynamics, spatial organization,
100 and secretory activity. We also study how the initial bacterial density influences the growth
101 pattern and activity of embedded bacteria, demonstrating the possibility to tune the secretory
102 kinetics to obtain prolonged activity.

103 **Results and Discussion**

104 **Influence of rigidity of the embedding matrix on bacterial growth**

105 We first aimed to study how embedded bacterial cells respond to the mechanical constraints
106 imposed by the surrounding physical hydrogel, with a focus on sustaining their proliferation
107 and activity. For this, two gram-positive, non-motile bacterial strains differing in shape, namely
108 *S. epidermidis* engineered to express green fluorescent protein (denoted GFP-*S. epidermidis*)
109 and *L. plantarum* expressing mScarlet (denoted mScarlet-*L. plantarum*), were selected.
110 Additionally, different nutrient-enriched physically-crosslinked agarose hydrogels were
111 prepared to embed these bacteria (Table 1), differing in their agarose concentration (from 0.5
112 to 2.0%) or in their agarose grades (ultra-low gel strength "UL-agarose", low gel strength "L-
113 agarose", and high gel strength "H-agarose"). Rheological measurements were performed on
114 the agarose hydrogel formulations to obtain their storage (G′) and loss (G″) moduli (Fig. S1,
115 Supplementary Information), confirming a wide range of mechanical properties between these
116 three grades (Table 1): the storage modulus (G') increased from 32 Pa for 1.0% UL-agarose to
117 1200 Pa for 1.0% L-agarose, with the storage modulus of the 1.0% H-agarose hydrogel even
118 not being accurately measurable due to its much higher rigidity.

119

**Table 1**. Description of the agarose hydrogels prepared in Difco™ Nutrient broth and their corresponding rheological characteristics at 37 °C under a stress amplitude of 1 Pa and a frequency of 1 Hz.

| | UL-agarose | | L-agarose | | H-agarose (*) | |
|---|---|---|---|---|---|---|
| Concentration (% w/v) | 1.0 | 0.5 | 1.0 | 2.0 | 1.0 | 1.5 |
| Storage modulus G' (Pa) | 32 | 310 | 1200 | 1600 | - | - |
| Tan$\delta$ | 0.06 | 0.03 | 0.05 | 0.08 | - | - |

(*) This hydrogel was too strong to be measured with accuracy.

To evaluate how matrix rigidity modulates bacterial behavior, we embedded GFP-*S. epidermidis* and mScarlet-*L. plantarum* in agarose hydrogels. We first worked with L-agarose hydrogels of increasing polymer concentrations (0.5%, 1.0%, and 2.0% w/v). By working with a single grade of agarose, we avoid possible complexities associated to the changing composition of the macromolecules in the different grades. Besides, the variation of tested concentrations alone provides a wide range of storage moduli, from 310 to 1600 Pa (Table 1). This increase of rigidity reflects the progressive densification of the agarose macromolecular network with higher polymer concentration, resulting in stronger gels of reduced deformability [38,47–50].

Fig. 1A shows optical microscopy images of spherical GFP-*S. epidermidis* cells embedded in these hydrogels, recorded at various culture times. In contrast to liquid culture in which the cells are homogeneously distributed throughout the volume (Fig. S2, Supplementary Information), proliferation within hydrogels led to the formation of multicellular aggregates. The formation of bacterial aggregates into both physical and chemical hydrogels has been extensively reported [16,17,29,51,52] and is generally attributed to the mechanical constraints imposed by the matrix, which prevent growing cells from easily moving away after division. Regardless of the

L-agarose concentration, proliferation appeared to initiate from a single cell and proceeded in a concentric manner, with aggregates expanding radially from the center. However, after 24 hours of culture, aggregate size no longer increased in our agarose systems, likely due to nutrient depletion in the medium, which led to growth arrest. The effect of matrix rigidity on aggregate architecture becomes increasingly apparent as cell proliferation progresses and aggregates grow. As summarized schematically in Fig. 1B, increasing L-agarose concentration led to progressively more compact and organized aggregates. At 0.5%, aggregates remained fuzzy with no clear boundary, while at 1.0% they became spherical with well-defined boundaries. At 2.0%, part of bacterial aggregates adopted a lenticular morphology, likely reflecting increased mechanical resistance to radial expansion. Although we did not explore stiffer agarose conditions beyond 2.0%, studies using chemically cross-linked hydrogels, such as Pluronic diacrylate-based matrices, have shown that bacterial aggregate expansion can be inhibited under highly elastic and non-deformable environments [29,31,32].

The pore size of agarose gels was shown to increase towards the micrometer range at low concentrations, approaching the size of cells. Together with local rearrangement of the macromolecular network arising from the pressure exerted by growing cells, this permits easier diffusion of bacteria through the agarose, resulting in a more fuzzy boundary at low gel concentrations [53,54]. Thus, the observed morphological transition from fuzzy to compact aggregates reflects the decreasing capacity of the agarose hydrogel to deform under the pressure exerted by growing cells. Indeed, unlike covalently cross-linked hydrogels with predominantly elastic behavior, agarose can undergo local rearrangements of its fibrillar network due to reversible physical cross-links, allowing for matrix relaxation and adaptation to growing cellular masses [50,55].

The viscoelastic properties of the embedding matrix modulate bacterial aggregate morphology but intrinsic cellular traits may also contribute to their organization. Previous studies have demonstrated that bacterial cell shape can play a selective role in growth dynamics under physical confinement by influencing aggregate architecture [56]. Rod-shaped bacteria were shown to form more elongated aggregates with increased surface area, thereby facilitating enhanced nutrient accessibility, in contrast to the more compact spherical aggregates typically formed by spherical bacteria. These findings motivated us to examine whether cell shape also impacts aggregate organization in agarose hydrogels. To this end, we performed parallel experiments with rod-shaped mScarlet-*L. plantarum* embedded in 0.5%, 1.0%, and 2.0% L-agarose. Although the mechanical properties of these L-agarose hydrogels differed slightly from those used for GFP-*S. epidermidis*, owing to the use of a different culture broth (Table S1, Supplementary Information), both strains exhibited similar qualitative patterns across agarose concentrations, as shown in the 3D reconstructed confocal images recorded after 24 hours (Fig. 1C): increasing rigidity led to more compact and organized aggregates, with lenticular shapes occasionally emerging at the higher agarose concentration. These results suggest that matrix mechanics dominate over intrinsic cellular shape in determining aggregate morphology, at least within this range of rigidities.

While spatial structure is clearly affected, it remains unclear whether this morphological reorganization of bacterial aggregates across gel rigidity translates into altered bacterial metabolism. Beyond purely geometric features, aggregate structure may influence the local microenvironment experienced by embedded cells. In particular, the spatial arrangement of bacteria within aggregates likely exposes the cells to heterogeneous gradients of oxygen, nutrients, and quorum-sensing molecules, which may modulate gene expression and, in turn, affect bacterial growth, function and metabolism. To address this, we quantified bacterial

growth kinetics using fluorescence intensity as an indirect measure for biomass accumulation and fitted the resulting curves using Richards' model [57]. As shown in Fig. 1D and 1E, both GFP-*S. epidermidis* and mScarlet-*L. plantarum* exhibited nearly identical growth dynamics across the three gel concentrations. The extracted maximal relative growth rates ($\mu_{rel}$) showed no significant differences, indicating that proliferation is not impacted by increased matrix rigidity, despite pronounced differences in aggregate structure. This suggests that the growth and activity of these bacteria are robust to changes in mechanical confinement within physically cross-linked agarose systems.

Having established that growth rates remain unchanged with gel strength, we next examined whether aggregate size is affected by gel rigidity. Quantification of the projected surface area of aggregates after 24 hours revealed no significant variation across agarose concentrations (Fig. 1F), further supporting the idea that overall biomass accumulation is insensitive to increasing confinement. While the projected area remained stable for both strains, aggregate circularity increased whereas roundness remained globally constant with gel rigidity (Fig. 1G and 1H). Circularity is the ratio between the area of the object and the one of a perfect circle of same perimeter, while roundness is the ratio between the area of the object and that of a circle having the same major axis length. Unlike circularity, which is based on the object's perimeter and is sensitive to contour irregularities, roundness reflects overall elongation and is less affected by edge roughness. An increase of circularity together with a constant roundness indicates a reduction in boundary complexity with increasing gel rigidity, rather than a change in the large-scale shape of the aggregates. Quantitative image analysis further revealed that circularity values were systematically higher for *S. epidermidis* than for *L. plantarum*, reflecting the inherently more symmetrical shape of spherical cells compared to rod-shaped ones. In contrast, the fact that roundness remained unchanged across bacteria and conditions suggests

that the mechanical constraints imposed by the tested agarose concentrations were not sufficiently strong to induce a significant elongation effect dependent on bacterial shape. As observed previously, only a fraction of lenticular aggregates was present in the stiffest gel condition, contributing very little to the overall roundness values. Overall, our results highlight that the mechanical environment governs the overall time-dependence of aggregate organization, with little influence of bacterial shape.

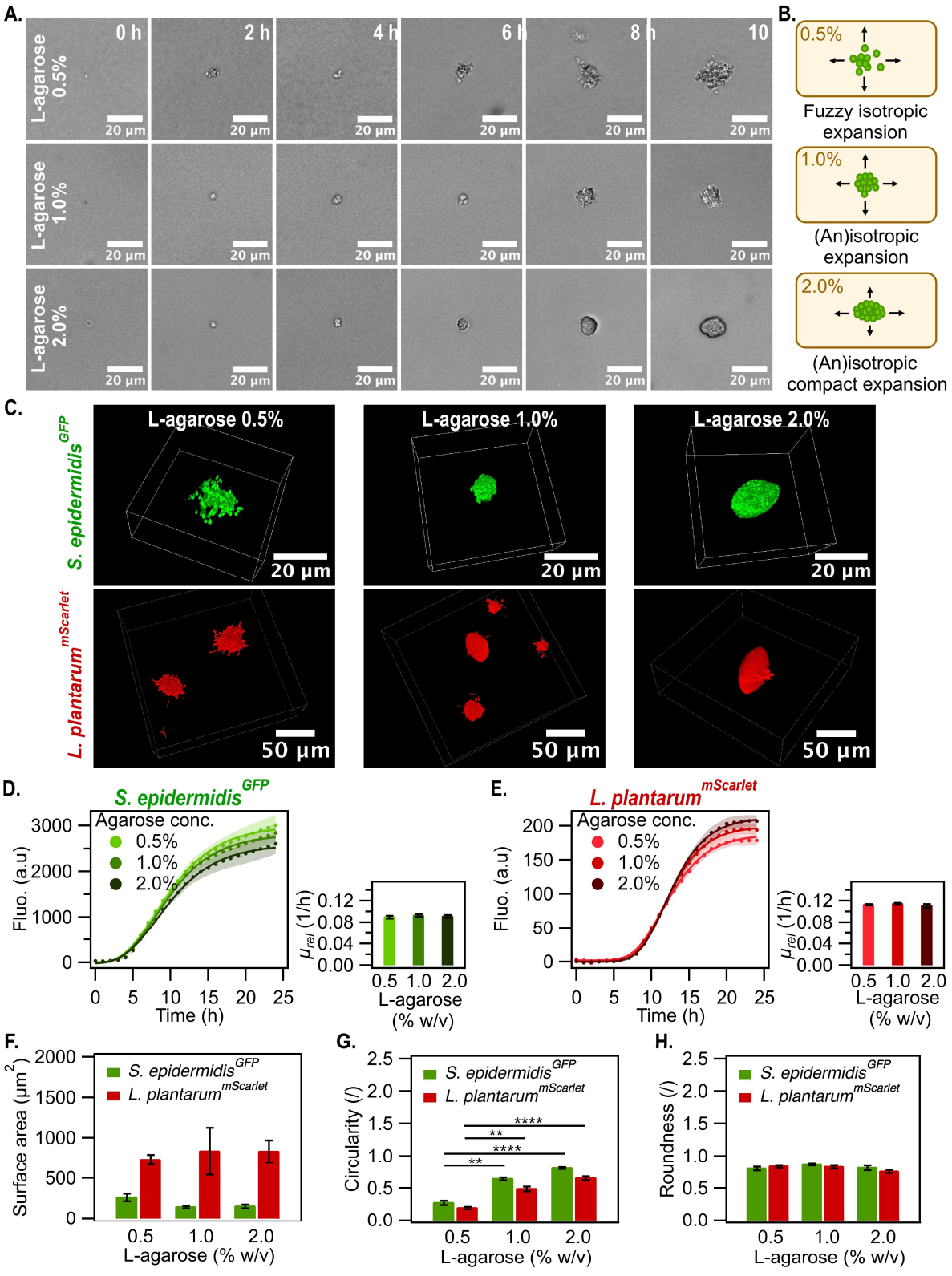


**Fig. 1.** Influence of agarose concentration on GFP-*S. epidermidis* and mScarlet-*L. plantarum* growth. **A.** Time-lapse brightfield microscopy images showing representative *S. epidermidis* aggregates formed in 0.5%, 1.0%, and 2.0% L-agarose gels. **B.** Schematic representation of the proliferation patterns observed as a function of increasing agarose gel rigidity. **C.** 3D confocal microscopy images of bacterial aggregates, recorded in L-agarose gels with

different concentrations, after 24 hours of culture. **D-E.** Bacterial growth curves fitted with the Richards' model, along with the maximal relative growth rates ($\mu_{rel}$) extracted from these curves (green: GFP-*S. epidermidis*; red: mScarlet-*L. plantarum*). The relative growth rate was calculated by dividing the absolute growth rate by the growth amplitude obtained from the growth curves. Data in **D-E** correspond to $N = 2$ independent experiments, $n = 5$ for *S. epidermidis* and N=3 independent experiments, $n = 3$ for *L. plantarum*. **F-H.** Quantitative analysis of morphological parameters of both strains grown in L-agarose gels at different concentrations (green bars: GFP-*S. epidermidis*; red bars: mScarlet-*L. plantarum*). Measurements were performed on maximum intensity projections of 3D confocal images from approximately 10 to 20 aggregates per condition in a single representative experiment: **F.** average surface area, **G.** circularity and **H.** roundness of the projected surface of bacterial aggregates. Statistical significance was assessed using the Kruskal-Wallis test followed by Dunn's multiple comparisons post-hoc test, with $^{**}p < 0.01$ and $^{****}p < 0.0001$.

However, in their natural environments, bacterial communities are rarely shaped by physical forces alone. Many species produce an extracellular matrix that plays a central role in maintaining aggregate integrity and biofilm architecture. This matrix could potentially enhance or counteract the effects of mechanical confinement, particularly in soft environments. To explore the influence of matrix production on aggregate morphology, we turned to a comparison between wild-type GFP-*S. epidermidis* and a mutant strain lacking the ica operon and therefore deficient in biofilm formation. Both strains formed similarly shaped aggregates across all tested L-agarose concentrations (Fig. S3, Supplementary Information), indicating that in those agarose systems, the formation and morphology of bacterial aggregates are primarily governed by the mechanical constraints imposed by the hydrogel matrix, rather than by extracellular matrix components such as exopolysaccharides (EPS). It is worth noting that our results align with those of Staudinger et al. [52], who also observed aggregate formation of biofilm-deficient *P. aeruginosa* mutants growing in agar hydrogels. *Listeria monocytogenes* and *Escherichia coli* which have very different secretion systems compared to *S. epidermidis* and *L. Plantarum* showed similar aggregate morphology when cultured in agarose gel [58].

This suggests that neither cell shape nor cell secretions significantly influence aggregate morphology or growth, whereas the mechanical environment emerges as the dominant factor. Until now, we modulated gel rigidity by varying agarose concentration. However, this approach does not account for other physicochemical properties of the gel (*i.e.*, variations in molar mass, degree of substitution, and chain conformation leading to distinct network architectures) that may also influence bacterial behavior. While polymer concentration is a well-established parameter to control hydrogel rigidity, different commercial grades of agarose, defined by their gel strength, exhibit distinct rheological behaviors even at identical concentrations (Table 1). To assess whether such variations in agarose grade impact bacterial growth and organization in a manner akin to concentration-dependent changes, we compared three agarose grades, namely ultra-low (UL), low (L) and high (H) strength gels. As shown in Fig. 2A, increasing gel strength by selecting the agarose grade led to more compact and lenticular aggregates, mirroring the effects observed with increasing concentration. Growth kinetics based on fluorescence measurements (Fig. 2B and 2C) showed only minor differences across agarose grades, confirming that matrix rigidity influences morphology but not bacterial proliferation. This reinforces the idea that aggregate shape is governed by mechanical constraints, regardless of how they are introduced, either by increasing polymer content or by changing the physicochemical nature of the gel.

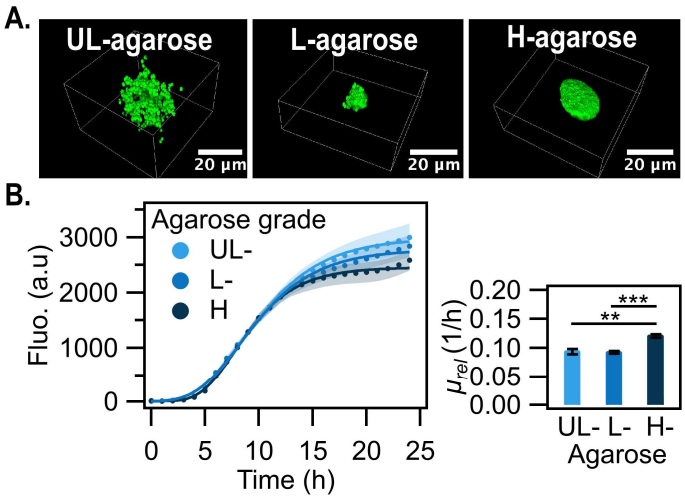


**Fig. 2.** Influence of agarose grades on GFP-*S. epidermidis*. **A.** 3D confocal microscopy images showing GFP-*S. epidermidis* aggregates in different grades of agarose (UL-, L-, and H-agarose), prepared at the same concentration (1.0% w/v). Images were taken after 24 hours of culture. **B.** Bacterial growth curves fitted with the Richards' model, along with the maximal relative growth rates extracted from the curves ($N = 2$, $n = 5$). Statistical analyses were performed using Kruskal-Wallis test with Dunn's post-hoc comparisons. Significance is indicated as $^{**}p < 0.01$, $^{***}p < 0.001$.

## Influence of initial bacterial density on bacterial growth in agarose gel

After having established the role of matrix rigidity in shaping bacterial aggregates, we turned our attention to the influence of initial bacterial density. While matrix mechanics constrain the physical space available for bacterial proliferation, the initial number of cells entrapped in the hydrogel determines how bacteria distribute and compete for limited resources. Moreover, cell-to-cell communication regulating bacterial proliferation and activity is a direct function of the population density [59]. For these reasons, we expected the initial bacterial density to affect both the biomass dynamics and the morphology of the resulting aggregates by modulating local nutrient consumption and quorum-sensing dynamics.

To evaluate this, rigid 1.5% H-agarose hydrogels were inoculated with GFP-expressing *S. epidermidis* at concentrations ranging from $10^3$ to $10^6$ CFU/mL. Biomass accumulation over time was first assessed by measuring total fluorescence across 48 hours. We observed that while

295 the lag phase duration was strongly dependent on the initial bacterial density, with high density
296 ($10^6$ CFU/mL) initiating growth after ~2 hours and low density ($10^3$ CFU/mL) showing delayed
297 growth up to ~9-10 hours, the subsequent exponential growth rates were comparable across
298 conditions (Fig. 3A). Furthermore, the final fluorescence levels at 48 hours reached comparable
299 plateaus, consistent with previous reports showing that under spatial and nutrient confinement,
300 final biomass tends to converge regardless of the initial bacterial density [60,61].
301 Despite similar biomass accumulation, confocal 3D reconstructions revealed strong differences
302 in aggregate morphology. Notably, increasing the initial bacterial density led to the formation
303 of smaller, more numerous aggregates (Fig. 3B). A quantitative analysis of the equatorial cross-
304 sections of individual aggregates confirmed a significant and exponential reduction in aggregate
305 size with increasing initial bacterial density (Fig. 3C), in line with observations reported for
306 other bacterial species embedded in agar [62], agarose [51], alginate [61] or food-type matrices
307 [60,63]. This size reduction likely stems from increased local competition for nutrients at high
308 initial bacterial density, which limits the proliferation of cells within individual aggregates.

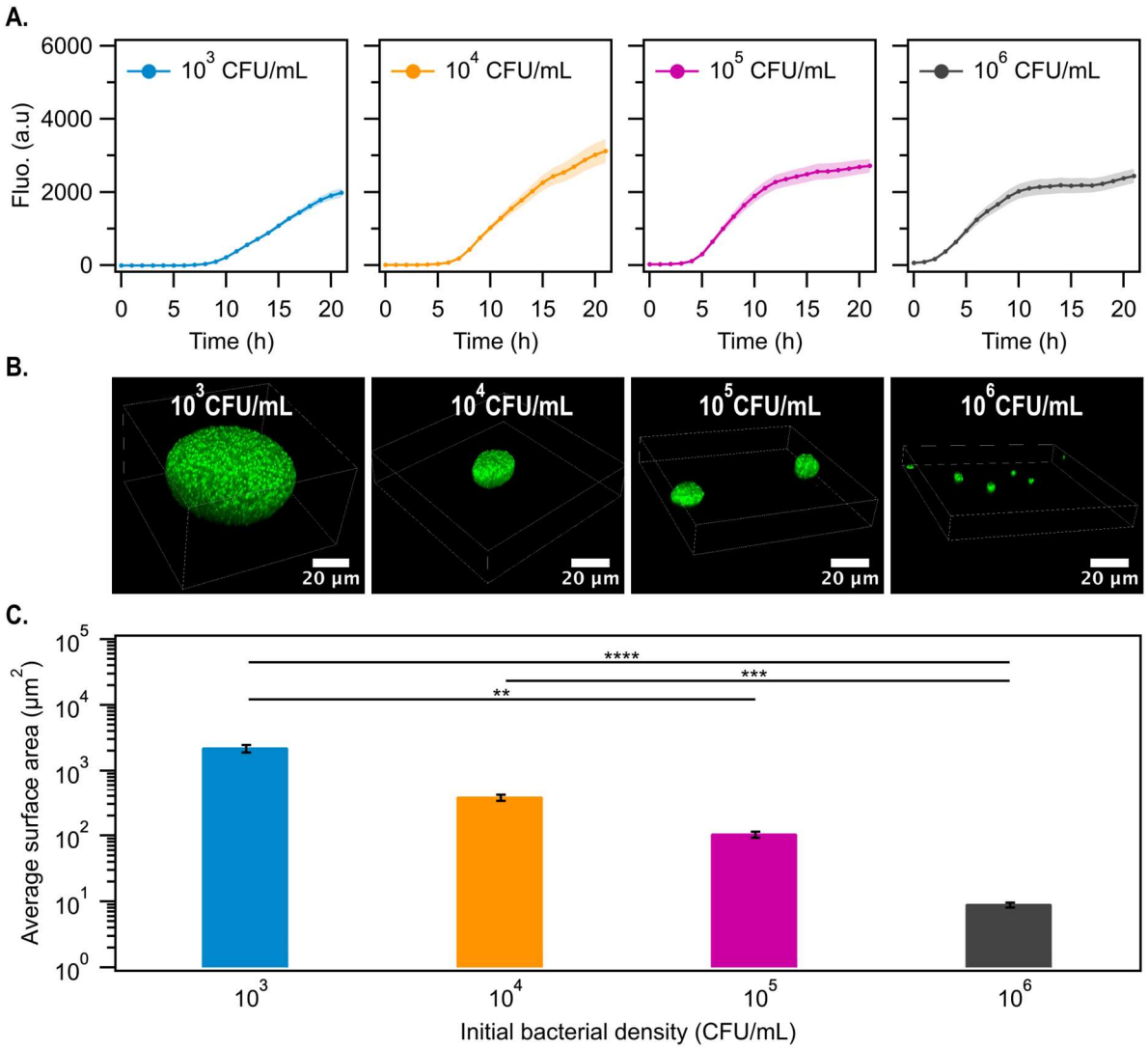


**Fig. 3.** Influence of initial bacterial density on the growth kinetics and morphodynamics of GFP- *S. epidermidis* in a rigid H-agarose gel (1.5% w/v). **A.** Growth curves corresponding to different initial bacterial densities, ranging from $10^3$ to $10^6$ CFU/mL ($N = 2$, $n = 5$). **B.** 3D confocal microscopy images of bacterial aggregates formed at each initial bacterial density, acquired after 24 h of culture. **C.** Quantification of the average surface area of approximately 10-20 aggregates measured in the equatorial plane after 24 hours of culture, in a single representative experiment. Statistical analyses were performed using Kruskal-Wallis test with Dunn's post-hoc comparisons. Significance is indicated as $^{**}p < 0.01$, $^{***}p < 0.001$, $^{****}p < 0.001$.

To broaden the scope of our study, we extended the analysis to mScarlet-*L. plantarum* and included additional matrix conditions by testing three L-agarose concentrations (0.5%, 1.0%, and 2.0%). Despite differences in gel stiffness, we again observed that initial bacterial density

primarily influenced the lag phase duration, while the final biomass remained similar across conditions. For clarity and because growth curves were similar across all three rigidities, only the data from the 2.0% agarose gel, including growth curves and confocal images, are shown in Fig. 4A and 4B. Aggregate size decreased with increasing initial bacterial density, consistent with the trend seen in GFP-*S. epidermidis*.

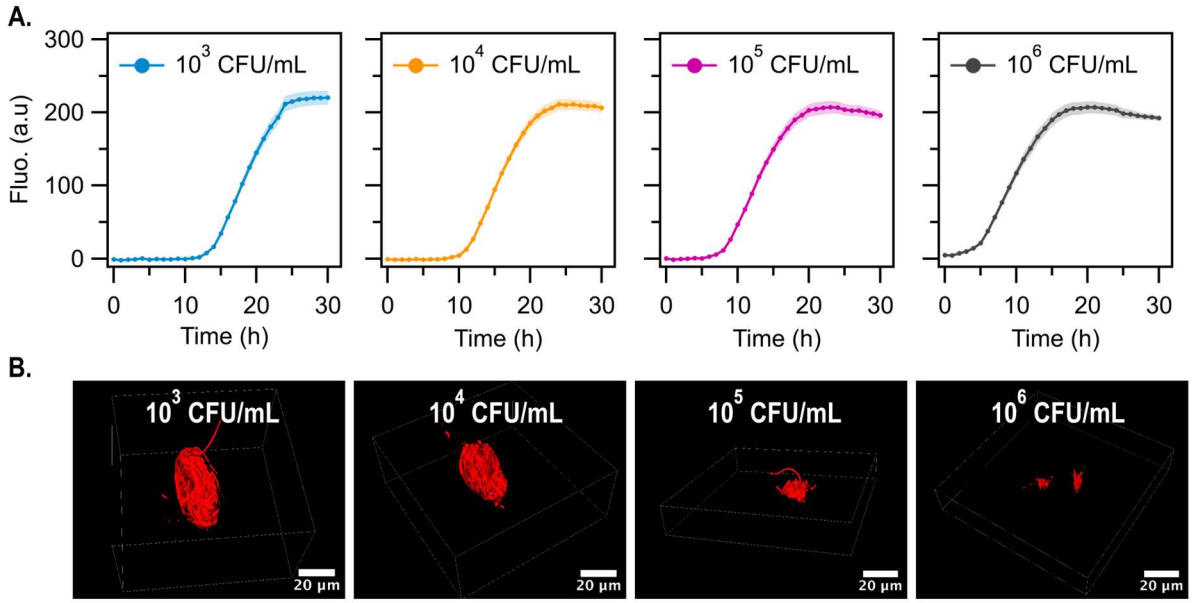


**Fig. 4.** Influence of initial bacterial density on the growth kinetics and morphodynamics of mScarlet-*L. plantarum* in 2.0% L-agarose gel. **A.** Growth curves corresponding to different initial bacterial densities, ranging from $10^3$ to $10^6$ CFU/mL ($N = 3$, $n = 3$). **B.** 3D confocal microscopy images of *L. plantarum* aggregates formed at each initial bacterial density, acquired after 24 hours of culture.

## Influence of cellular organization in the gels on the secretory activity

Matrix rigidity and initial bacterial density are key parameters that influence the spatial organization and physiological behavior of bacteria embedded in hydrogels. While rigidity primarily controls aggregate morphology, initial bacterial density modulates aggregate size, thereby tuning the microenvironmental conditions experienced by bacterial populations. Additionally, aggregate size in turn impacts local gradients of nutrients and secreted metabolites, which could explain delayed growth for the lower initial bacterial densities as

suggested previously by other [58]. Given that such microenvironments can affect metabolism, we investigated how these two parameters impact the secretory activity of *L. plantarum* bacteria genetically modified to produce elafin (*L. plantarum*-elafin) [64] a protein with protease inhibitor properties [65].

To this end, *L. plantarum*-elafin was embedded in L-agarose hydrogels of varying rigidity (0.5%, 1.0%, and 2.0%) and inoculated at different concentrations ($10^3$ to $10^6$ CFU/mL). The resulting bacterial spatial organizations were characterized by microscopy after 24 hours (Fig. 5A), confirming the previously observed variations in aggregate size and distribution as a function of both gel concentration and initial bacterial density.

Secretory activity was systematically measured by performing an inhibition test in presence of neutrophil elastase and a fluorogenic peptide substrate. More precisely, elafin interacts with the neutrophil elastase to block its catalytic site, thereby preventing the access and cleavage of the fluorogenic substrate, thereby reducing the rate of production of a fluorescent probe. Therefore, the quantification of secreted elafin can be done through the decrease in the rate of fluorescence increase measured in the supernatant, slower rates indicating higher quantities of elafin. Initial measurements showed that matrix rigidity had no significant effect on elafin secretion and release, while initial bacterial density significantly influenced secretion levels after 24 h, with higher initial bacterial densities producing greater elastase inhibition (Fig. 5B).

To assess whether secretion was merely delayed or fundamentally impaired, we extended the duration of the assay on the L-agarose 2.0% and monitored neutrophil elastase inhibition over 72 hours (Fig. 5C). The results showed that low-initial bacterial density hydrogels eventually reached levels of secretory activity comparable to high-initial bacterial density conditions, albeit with a temporal delay. This indicates that bacterial aggregates, even when initially sparse and slow-growing, retain full secretory function once sufficient biomass is established. Therefore, the initial bacterial density modulates not the secretion capacity but rather the

kinetics of reaching it. This provides a very useful handle to control the release kinetics of bacterial therapeutic substances and consequently the release properties of the living hydrogels.

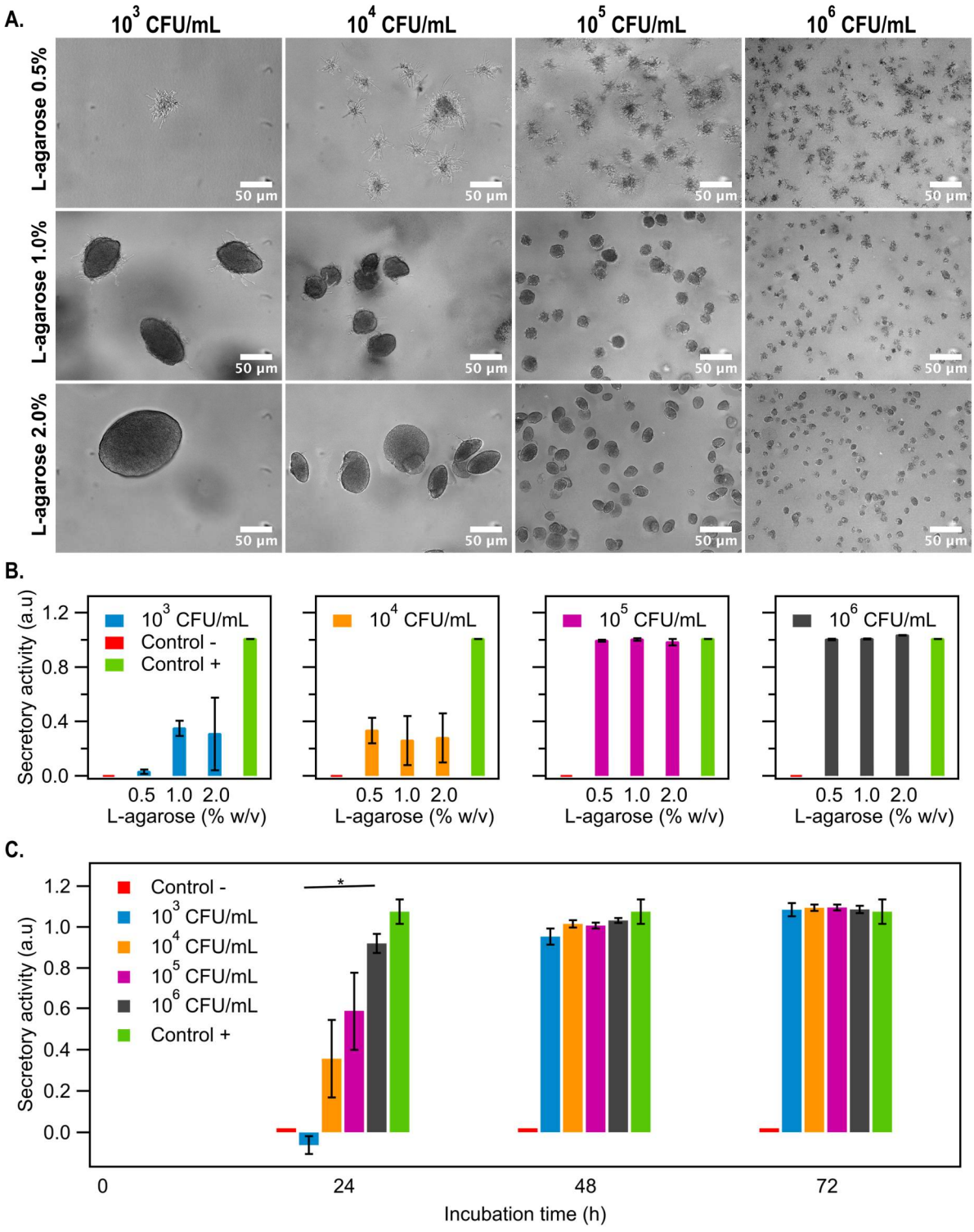


**Fig. 5.** Influence of gel rigidity and initial bacterial density on the secretory activity of *L. plantarum*-elafin. **A.** Brightfield microscopy images showing the cellular organization of *L. plantarum*-elafin aggregates after 24 hours of culture in L-agarose gels at different concentrations (0.5%, 1.0%, and 2.0% w/v) and initial bacterial densities

($10^3$ to $10^6$ CFU/mL). **B.** Secretory activity measured after 24 hours of culture, as a function of agarose concentration for each initial bacterial density (sterile MRS medium was used as negative control and the supernatant of a highly concentrated *L. plantarum* culture containing secreted elafin, was used as a positive control) ($N = 2$, $n = 1$). **C.** Effect of initial bacterial density on secretory activity measured after 24, 48, and 72 hours of culture in a 2.0% L-agarose ($N = 2$, $n = 2$). For each time, the data are displayed with the leftmost bar for the negative control, the rightmost bar for the positive control, and the intermediate bars for the four selected initial bacterial densities, from lowest to highest. Statistical analyses were performed using Kruskal–Wallis test followed by Dunn's post hoc test. Significance is set at $p < 0.05$ and indicated as * for $p < 0.05$.

## Conclusion

In this work, we systematically explored how two physical parameters, *i.e.*, matrix rigidity and initial bacterial density, influence the spatial organization and functional behavior of bacterial populations embedded in agarose hydrogels. We demonstrate that agarose rigidity effectively modulates aggregate morphology, influencing their shape and compactness within the matrix. In parallel, varying the initial bacterial density controls the temporal variation of the aggregate size. Together, these parameters offer complementary handles for engineering distinct microenvironments in 3D bacterial cultures. Importantly, we show that bacteria embedded in agarose gels maintain a robust growth and preserved secretory function across a wide range of embedding conditions, highlighting the suitability of agarose gels for sustaining active living systems. Importantly, initial bacterial density modulates the kinetics of both growth and secretory activity. Low initial densities lead to larger, spaced-out aggregates and slower biomass accumulation, resulting in delayed but not diminished secretory activity. Possible applications of this living hydrogel include therapeutic or cosmetic skin patches with sustained released of therapeutic bacterial molecules.

## Materials and Methods

### Materials

Three agarose grades with distinct gel strengths (Table 2) were purchased from Sigma-Aldrich: UL-agarose (Type IX), L-agarose (Type VII), and H-agarose (Type II-A). Difco™ Nutrient Broth (234000) was obtained from BD Diagnostics, while MRS broth (X925.2) was purchased from Carl Roth. Chloramphenicol (C0378) and erythromycin (E5389) were both obtained from Sigma-Aldrich and used as selective antibiotics in bacterial cultures. For the secretory activity assays, human neutrophil elastase (324681) was acquired from Sigma-Aldrich and the fluorogenic substrate N-(methoxysuccinyl)-alanine-proline-valine-7-amino-4-trifluoromethylcoumarin (MeOSuc-AAPV-AFC) (ab142178) was obtained from Abcam. Human neutrophil elastase (Sigma-Aldrich, 324681) was reconstituted in assay buffer (200 mM Tris-HCl, 200 mM NaCl, 0.05% Tween 20, 0.01% BSA, pH 7.5) to prepare a 200 µg/mL (200 ng/µL) stock solution, aliquoted and stored at −80 °C. The fluorogenic substrate N-(methoxysuccinyl)-Ala-Pro-Val-AMC was dissolved in DMSO to obtain a 2 mM stock solution, aliquoted and stored at −20 °C. Fluorescent strains *S. epidermidis* 1457 and its isogenic Δica mutant [66], both carrying the plasmid pCM29 (PsarA::sGFP, $cam^{(R)}$), were kindly provided by Prof. A. Horswill (University of Colorado School of Medicine, USA).

Two engineered strains of *L. plantarum* WCFS1 were employed in this study: a fluorescent strain harboring pTec_mScarlet, used for imaging, and a non-fluorescent strain carrying pTlpa_sp3_elafin, both with erythromycin selection marker was used to assess secretory activity. Both these genetic constructs were obtained using direct cloning method described in [67].

**Table 2**. Characteristics of the agarose grades used in this study as described by the provider.

| Name | Type(*) | Gel strength(*) [g.cm$^{-2}$] |
|---|---|---|
| UL-agarose | IX | ≥ 75 at 2.0% |
| L-agarose | VII | ≥ 200 at 1.0% |
| H-agarose | II-A | ≥ 1000 at 1.0% |

(*) According to the provider.

**Preparation of agarose hydrogels**

All powdered agarose types were directly mixed with dehydrated culture medium, followed by the addition of Milli-Q water. The quantities of agarose, culture medium powder, and Milli-Q water were adjusted to achieve the desired final concentrations of agarose (Table 1) and broth (8 g/L for BD broth and 52 g/L for MRS broth) in the gels. The resulting mixtures were then sterilized by autoclaving.

**Bacterial culture**

GFP-*S. epidermidis* was cultured in Difco™ Nutrient Broth supplemented with 10 µg/mL chloramphenicol and *L. plantarum* in MRS broth supplemented with 10 µg/mL. Cryo-preserved strains were revived overnight in 8 mL of broth in vented culture tubes incubated at 37°C and shaken at180 rpm and 250 rpm for GFP-*S. epidermidis* and *L. plantarum*, respectively. The resulting overnight precultures were used to inoculate fresh medium under the same conditions, and cells were grown for about 4-5 hours until reaching mid-exponential phase ($OD_{540}$ ~0.5 for GFP-*S. epidermidis* and $OD_{600}$ ~1.0 for *L. plantarum*). To determine the bacterial density, serial dilutions of cultures obtained at the target OD value were prepared and plated on agar using the single plate-serial dilution spotting (SP-SDS) method [68]. Plates were incubated at 37 °C for

48 hours, after which colonies were counted to calculate colony-forming units per milliliter (CFU/mL).

**Bacterial encapsulation in agarose hydrogels**

A bacterial suspension obtained from mid-exponential phase culture ($OD_{540}$ ~0.5 for GFP-*S. epidermidis* and $OD_{600}$ ~1.0 for *L. plantarum*) was diluted in fresh culture broth to the desired concentration. A volume of 0.5 mL of this diluted suspension was mixed in a sterile Eppendorf tube with 1 mL of concentrated agarose solution (tempered to ~40 °C), resulting in 1.5 mL of gel embedding bacteria. The concentration of the agarose solution was adjusted to get the desired concentration in the final mixture. The obtained mixture was then immediately transferred into the appropriate support (*e.g.*, 96-well microplate, Lab-Tek chamber, stage top chamber or Interactive Co-Culture Plate), depending on the intended experiment. To ensure complete gelation, samples were placed at 4 °C for 10 minutes before incubation at 37 °C. Unless otherwise specified, no additional nutrients were added beyond those initially present in the agarose hydrogel.

**Rheology**

Rheological measurements were performed on hydrogels prepared in broth, using a controlled stress rheometer (DHR2, TA Instrument, U.K.). Measurements were conducted with a striated plate-plate geometry (diameter 40 mm). Agarose solutions were heated to 85 °C for 30 minutes to reach a viscous liquid state then deposited on the Peltier plan heated to 50°C and the geometry gap was adjusted to 150 µm. The following protocol was subsequently followed to equilibrate the sample in temperature at a stress amplitude of 0.1 Pa and a frequency of 1 Hz: cooling from 50 to 10°C (2°C.min$^{-1}$), rest at 10°C for 20 minutes, heating from 10 to 37°C (2 °C.min$^{-1}$), rest at 37°C for 2 hours. All measurements were performed with a solvent trap to prevent

evaporation. The analysis of the data was performed with TRIOS V 5.1.0.46403 rheology software (TA Instrument, U.K.).

**Microscopy observation**

Bacteria-embedded agarose gels were imaged in bright-field mode using an Olympus IX71 inverted microscope equipped with a 40× dry objective and a stage-top incubator (Okolab, O-CT-UNO-TEMP-CO2), which maintained a constant temperature of 37 °C and humidity throughout the acquisition period. Imaging was conducted over 10 h, with manual image capture performed hourly. For each experimental condition, representative bacterial aggregates were selected and imaged at each time point.

After 24 hours of culture, three-dimensional reconstructions of bacterial aggregates within the hydrogels were obtained using Z-stacks on a laser-scanning confocal microscope (Stellaris DMI8 LEICA WLL–equipped with a HC PL APO 63x/1.20 W objective). Excitation and emission wavelengths were adjusted according to the fluorescent strains used (GFP-*S. epidermidis* and mScarlet-*L. plantarum*). The 3D images were processed with Lax X 3D visualization software.

Maximum intensity projections were generated for each stack to obtain a single-plane representation of the entire aggregate, which was then analyzed using ImageJ. Before measurement, images were preprocessed in ImageJ to improve segmentation quality. For each condition (agarose gel rigidity and bacterial strain), 10 to 20 representative aggregates were selected based on their frequent occurrence and representative morphology. Aggregates partially overlapping with another aggregate or for which segmentation failed were excluded. Circularity was used to quantify both aggregate shape and contour irregularity, ranging from 0

(highly elongated or irregular) to 1 (perfect circle). As additional metric, roundness was measured, reflecting the isotropic character of the structure and being less sensitive to contour irregularities than circularity. Values close to 1 indicate a structure that is uniform and isotropic, whereas values approaching 0 correspond to highly anisotropic or elongated aggregates.

**Study of bacterial growth kinetics**

Growth kinetics and biomass evolution were monitored in 96-well microplates containing 200 µL of agarose gel embedding bacteria, prepared as described above. Experiments were performed for the two bacterial strains (GFP-*S. epidermidis* and mScarlet-*L. plantarum*) under three types of conditions: varying initial bacterial density in a single agarose hydrogel composition, varying gel rigidity at a fixed initial bacterial density, and varying both initial bacterial density and gel rigidity simultaneously. Empty wells were filled with autoclaved water to prevent evaporation, and the plate was sealed with a sterile SealPlate film to maintain constant humidity. The microplates were incubated at 37 °C, and fluorescence intensity was recorded every hour until reaching the stationary phase, indicating the end of bacterial growth (excitation/emission: 488/515 nm for GFP, 569/635 nm for mScarlet). Background fluorescence from cell-free gels was subtracted to isolate the bacterial signal, and the resulting curves were fitted using the explicit form of the Richards model, which describes growth with five parameters [57]:

$$y = B + A\left\{1 + \nu \cdot \exp(1+\nu) \cdot exp\left[\mu_{rel} \cdot (1+\nu)^{(1+1/\nu)} \cdot (\lambda - t)\right]\right\}^{(-1/\nu)} \quad (1)$$

the background signal $B$, the asymptote ($A$) representing the maximum fluorescence reached above the background level, the maximal relative growth rate ($\mu_{rel}$) corresponding to the slope at the inflection point for the growth curve normalized to unit amplitude, the lag time ($\lambda$) defined as the intercept of the tangent of highest slope with the background level $B$, and $\nu$, a shape

parameter with no biological interpretation. Each gel condition was tested in two independent experiments, with at least three replicates per experiment. The average value of each extracted parameter was computed across all replicates.

**Study of secretory activity**

Agarose gel embedding *L. plantarum* secreting elafin were poured into the first chamber of an Interactive Co-Culture Plate (ICCP) (Xceltis, 2501-02AB) as described above. This commercial system consists of two adjacent chambers separated by a sterile semi-permeable track-etched polycarbonate membrane (pore density: $10^8$ $cm^{-2}$, pore diameter: 0.2 µm, membrane thickness: 25 µm, provided by it4ip S.A., Belgium), which retains bacteria in the first chamber while allowing diffusion of secreted molecules into the second chamber. The second chamber was filled with sterile MRS broth. The ICCP was incubated at 37 °C for 24 h. The next day, the content of the second container (MRS w/o bacteria) of the ICCP system was harvested and used for elafin detection.

This detection was carried out by evaluating the inhibitory activity of elafin against human neutrophil elastase in the presence of a fluorogenic peptide substrate, *N*-(methoxysuccinyl)-alanine-proline-valine-7-amino-4-trifluoromethylcoumarin. Upon cleavage by neutrophil elastase, the substrate releases 7-amino-4-trifluoromethylcoumarin, a fluorescent compound detectable using a spectrophotometer (excitation/emission: 380/460 nm). Experimentally, 50 µL of sample (supernatant collected from the ICCP second compartment) was mixed with 25 µL of neutrophil elastase (2 ng/µL in Tris-HCl buffer) and incubated for 5 minutes at 37 °C. Then, 25 µL of the fluorogenic substrate (0.1 mM in DMSO) was added in the dark. Fluorescence was monitored over 55 min at 37 °C in a microplate reader (Tecan Infinite 200 PRO). Secretory activity was quantified as follows, based on the slope of the fluorescence intensity versus time determined between 30 and 55 minutes:

$$Secretory\ activity = \frac{slope(negative\ control) - slop\ \ (sample)}{slope\ (negative\ control)} \quad (2)$$

A sterile MRS solution was used as negative control (no neutrophil elastase inhibition, high rate of fluorescence increase), and the supernatant of a highly concentrated *L. plantarum* culture (releasing a high enough content of elafin to fully inhibit the elastase activity) was used as a positive control (total neutrophil elastase inhibition, low rate of fluorescence increase due to residual activity). The secretory activity varies from 0 when the activity is identical to the negative control, to ~1 when the activity is similar to the one of the positive control.

**Statistical analysis**

Data are presented as mean ± standard error of the mean (SEM) unless otherwise specified. Statistical comparisons among multiple groups were conducted using the non-parametric Kruskal-Wallis test, followed by Dunn's post hoc test when the overall test was significant ($p < 0.01$). For the analysis of secretory activity, statistical significance was defined at $p < 0.05$ due to the limited sample size and high variability, which could reduce the statistical power of the test. All statistical analyses were performed using Python.

**CRediT author statement**

**L. Dupont**: Conceptualization, Methodology, Investigation, Formal analysis, Visualization, Writing - Original Draft. **V. S. Tadimarri**: Resources, Methodology, Writing - Review & Editing. **R. Buret**: Methodology, Investigation, Writing - Review & Editing. **S. Sankaran**: Writing - Review & Editing. **L. Picton**: Methodology, Writing - Review & Editing. **A. M. Jonas**: Supervision, Conceptualization, Writing - Review & Editing, Funding acquisition. **K. Glinel**: Supervision, Conceptualization, Writing - Review & Editing, Funding acquisition.

**Acknowledgments**

The authors thank it4ip S.A. (Belgium) for track-etched polycarbonate membranes and M.-C. Eloy (UCLouvain, Belgium) for her help with CLSM measurements. Prof. A. Horswill and Dr. J. Kavanaugh (University of Colorado School of Medicine, USA) are thanked for kindly providing the *S. epidermidis* strains. This work is supported by UCLouvain and ARC BACTOCIRCUIT (n°22/27-120).

**References**

[1] S. Yu, H. Sun, Y. Li, S. Wei, J. Xu, J. Liu, Hydrogels as promising platforms for engineered living bacteria-mediated therapeutic systems, Mater. Today Bio 16 (2022) 100435. https://doi.org/10.1016/j.mtbio.2022.100435.

[2] A.M. Jonas, K. Glinel, A. Behrens, A.C. Anselmo, R.S. Langer, A. Jaklenec, Controlling the growth of staphylococcus epidermidis by layer-by-layer encapsulation, ACS Appl. Mater. Interfaces 10 (2018) 16250–16259. https://doi.org/10.1021/acsami.8b01988.

[3] Q.W. Chen, X.Z. Zhang, Living biomaterials: Fabrication strategies and biomedical applications, Acc. Mater. Res. 5 (2024) 1440–1452. https://doi.org/10.1021/accountsmr.4c00258.

[4] Y. Jeong, J. Irudayaraj, Hierarchical encapsulation of bacteria in functional hydrogel beads for inter- and intra- species communication, Acta Biomater. 158 (2023) 203–215. https://doi.org/10.1016/j.actbio.2023.01.003.

[5] C. Lu, Y. Huang, J. Cui, J. Wu, C. Jiang, X. Gu, Y. Cao, S. Yin, Toward Practical Applications of engineered living materials with advanced fabrication techniques, ACS Synth. Biol. 13 (2024) 2295–2312. https://doi.org/10.1021/acssynbio.4c00259.

[6] A. Rodrigo-Navarro, S. Sankaran, M.J. Dalby, A. del Campo, M. Salmeron-Sanchez, Engineered living biomaterials, Nat. Rev. Mater. 6 (2021) 1175–1190. https://doi.org/10.1038/s41578-021-00350-8.

[7] V.H. Pérez-Luna, O. González-Reynoso, Encapsulation of biological agents in hydrogels for therapeutic applications, Gels 4 (2018). https://doi.org/10.3390/gels4030061.

[8] M. Mafi, A. Kushmaro, C. Greenblatt, S. Agarwal, A. Greiner, Poly(vinyl alcohol)-hydrogel microparticles with soft barrier shell for the encapsulation of micrococcus luteus, Macromol. Biosci. 21 (2021) e2000419. https://doi.org/10.1002/mabi.202000419.

[9] T.C. Tang, E. Tham, X. Liu, K. Yehl, A.J. Rovner, H. Yuk, C. de la Fuente-Nunez, F.J. Isaacs, X. Zhao, T.K. Lu, Hydrogel-based biocontainment of bacteria for continuous sensing and computation, Nat. Chem. Biol. 17 (2021) 724–731. https://doi.org/10.1038/s41589-021-00779-6.

[10] N. Ido, A. Lybman, S. Hayet, D.N. Azulay, M. Ghrayeb, S. Liddawieh, L. Chai, Bacillus subtilis biofilms characterized as hydrogels. Insights on water uptake and water binding in biofilms, Soft Matter 16 (2020) 6180–6190. https://doi.org/10.1039/d0sm00581a.

[11] A. Revete, A. Aparicio, B.A. Cisterna, J. Revete, L. Luis, E. Ibarra, E.A. Segura González, J. Molino, D. Reginensi, Advancements in the use of hydrogels for regenerative medicine: Properties and biomedical applications, Int. J. Biomater. 2022 (2022) 3606765. https://doi.org/10.1155/2022/3606765.

[12] L.M. González, N. Mukhitov, C.A. Voigt, Resilient living materials built by printing bacterial spores, Nat. Chem. Biol. 16 (2020) 126–133. https://doi.org/10.1038/s41589-019-0412-5.

[13] S. Sankaran, J. Becker, C. Wittmann, A. del Campo, Optoregulated drug Release from an engineered living material: Self-replenishing drug depots for long-term, light-regulated delivery, Small 15 (2019) 1804717. https://doi.org/10.1002/smll.201804717.

[14] H.H. Tuson, G.K. Auer, L.D. Renner, M. Hasebe, C. Tropini, M. Salick, W.C. Crone, A. Gopinathan, K.C. Huang, D.B. Weibel, Measuring the stiffness of bacterial cells from growth rates in hydrogels of tunable elasticity, Mol. Microbiol. 84 (2012) 874–891. https://doi.org/10.1111/j.1365-2958.2012.08063.x.

[15] B. Pabst, B. Pitts, E. Lauchnor, P.S. Stewart, Gel-entrapped Staphylococcus aureus bacteria as models of biofilm infection exhibit growth in dense aggregates, oxygen limitation, antibiotic tolerance, and heterogeneous gene expression, Antimicrob. Agents Chemother. 60 (2016) 6294–6301. https://doi.org/10.1128/AAC.01336-16.

[16] Q. Zhang, J. Li, J. Nijjer, H. Lua, M. Kothari, R. Alert, T. Cohen, J. Yan, Morphogenesis and cell ordering in confined bacterial biofilms, Proc. Natl. Acad. Sci. USA 118 (2021) e2107107118. https://doi.org/10.1073/pnas.2107107118/-/DCSupplemental.

[17] M. Antwi, A.H. Geeraerd, K.M. Vereecken, R. Jenné, K. Bernaerts, J.F. Van Impe, Influence of a gel microstructure as modified by gelatin concentration on Listeria innocua growth, Innov. Food Sci. Emerg. Technol. 7 (2006) 124–131. https://doi.org/10.1016/j.ifset.2005.08.001.

[18] T.E. Theys, A.H. Geeraerd, A. Verhulst, K. Poot, I. Van Bree, F. Devlieghere, P. Moldenaers, D. Wilson, T. Brocklehurst, J.F. Van Impe, Effect of pH, water activity and gel micro-structure, including oxygen profiles and rheological characterization, on the growth kinetics of Salmonella Typhimurium, Int. J. Food Microbiol. 128 (2008) 67–77. https://doi.org/10.1016/j.ijfoodmicro.2008.06.031.

[19] A. Dafe, H. Etemadi, H. Zarredar, G.R. Mahdavinia, Development of novel carboxymethyl cellulose/k-carrageenan blends as an enteric delivery vehicle for

638 probiotic bacteria, Int. J. Biol. Macromol. 97 (2017) 299–307.
639 https://doi.org/10.1016/j.ijbiomac.2017.01.016.
640 [20] D .Zapryana, A. Krastanov, I. Murgov, Immobilized lactic acid bacteria for application
641 as dairy starters and probiotic preparations, J. Gen. Appl. Microbiol. 50 (2004) 107-114.
642 https://doi: 10.2323/jgam.50.107. 2004.
643 [21] S. Guo, E. Dubuc, Y. Rave, M. Verhagen, S.A.E. Twisk, T. Van Der Hek, G.J.M.
644 Oerlemans, M.C.M. Van Den Oetelaar, L.S. Van Hazendonk, M. Brüls, B. V. Eijkens,
645 P.L. Joostens, S.R. Keij, W. Xing, M. Nijs, J. Stalpers, M. Sharma, M. Gerth, R.J.E.A.
646 Boonen, K. Verduin, M. Merkx, I.K. Voets, T.F.A. De Greef, Engineered living
647 materials based on adhesin-mediated trapping of programmable cells, ACS Synth. Biol.
648 9 (2020) 475–485. https://doi.org/10.1021/acssynbio.9b00404.
649 [22] K. Witte, A. Rodrigo-Navarro, M. Salmeron-Sanchez, Bacteria-laden microgels as
650 autonomous three-dimensional environments for stem cell engineering, Mater. Today
651 Bio 2 (2019) 100011. https://doi.org/10.1016/j.mtbio.2019.100011.
652 [23] K. Schulz-Schönhagen, N. Lobsiger, W.J. Stark, Continuous production of a shelf-stable
653 living material as a biosensor platform, Adv. Mater. Technol. 4 (2019) 1900266.
654 https://doi.org/10.1002/admt.201900266.
655 [24] M. Radosavljević, S. Lević, M. Belović, J. Pejin, A. Djukić-Vuković, L. Mojović, V.
656 Nedović, Encapsulation of Lactobacillus rhamnosus in polyvinyl alcohol for the
657 production of L-(+)-lactic acid, Process Biochem. 100 (2021) 149–160.
658 https://doi.org/10.1016/j.procbio.2020.10.006.
659 [25] T. Tantimongcolat, C. Isarankura-Na-Ayudhya, A. Srisarin, H.-J. Galla, V.
660 Prachayasittikul, Polyacrylamide hydrogel encapsulated E. coli expressing metal-
661 sensing green fluorescent protein as a potential tool for copper ion determination, EXCLI
662 J. 13 (2014) 401–415. https://www.excli.de/excli/article/view/706

[26] T.G. Johnston, S.F. Yuan, J.M. Wagner, X. Yi, A. Saha, P. Smith, A. Nelson, H.S. Alper, Compartmentalized microbes and co-cultures in hydrogels for on-demand bioproduction and preservation, Nat. Commun. 11 (2020) 563. https://doi.org/10.1038/s41467-020-14371-4.

[27] A. Saha, T.G. Johnston, R.T. Shafranek, C.J. Goodman, J.G. Zalatan, D.W. Storti, M.A. Ganter, A. Nelson, Additive manufacturing of catalytically active living materials, ACS Appl. Mater. Interfaces 10 (2018) 13373–13380. https://doi.org/10.1021/acsami.8b02719.

[28] S. Bhusari, J. Kim, K. Polizzi, S. Sankaran, A. del Campo, Encapsulation of bacteria in bilayer Pluronic thin film hydrogels: A safe format for engineered living materials, Biomater. Adv. 145 (2023) 213240. https://doi.org/10.1016/j.bioadv.2022.213240.

[29] S. Bhusari, S. Sankaran, A. del Campo, Regulating bacterial behavior within hydrogels of tunable viscoelasticity, Adv. Sci. 9 (2022) 2106026. https://doi.org/10.1002/advs.202106026.

[30] M. Lufton, O. Bustan, B. hen Eylon, E. Shtifman-Segal, T. Croitoru-Sadger, A. Shagan, A. Shabtay-Orbach, E. Corem-Salkmon, J. Berman, A. Nyska, B. Mizrahi, Living bacteria in thermoresponsive gel for treating fungal infections, Adv. Funct. Mater. 28 (2018) 1801581. https://doi.org/10.1002/adfm.201801581.

[31] S. Bhusari, M. Hoffmann, P. Herbeck-Engel, S. Sankaran, M. Wilhelm, A. del Campo, Rheological behavior of pluronic/pluronic diacrylate hydrogels used for bacteria encapsulation in engineered living materials, Soft Matter 20 (2023) 1320–1332. https://doi.org/10.1039/d3sm01119d.

[32] Y. Han, N. Jiang, H. Xu, Z. Yuan, J. Xiu, S. Mao, X. Liu, J. Huang, Extracellular matrix rigidities regulate the tricarboxylic acid cycle and antibiotic resistance of three-

dimensionally confined bacterial microcolonies, Adv. Sci. 10 (2023) 2206153. https://doi.org/10.1002/advs.202206153.

[33] R. Armisén, Agar and agarose biotechnological applications. Hydrobiologia 221 (1991) 157–166. https://doi.org/10.1007/BF00028372.

[34] F.B.A. Descallar, S. Matsukawa, Change of network structure in agarose gels by aging during storage studied by NMR and electrophoresis, Carbohydr. Polym. 245 (2020) 116497. https://doi.org/10.1016/j.carbpol.2020.116497.

[35] P. Zucca, R. Fernandez-Lafuente, E. Sanjust, Agarose and its derivatives as supports for enzyme immobilization, Molecules 21 (2016) 1577. https://doi.org/10.3390/molecules21111577.

[36] A. Irastorza-lorenzo, D. Sánchez-porras, O. Ortiz-Arrabal, M.J. de Frutos, E. Esteban, J. Fernández, A. Janer, A. Campos, F. Campos, M. Alaminos, Evaluation of marine agarose biomaterials for tissue engineering applications, Int. J. Mol. Sc.i 22 (2021) 1923. https://doi.org/10.3390/ijms22041923.

[37] P. Zarrintaj, S. Manouchehri, Z. Ahmadi, M.R. Saeb, A.M. Urbanska, D.L. Kaplan, M. Mozafari, Agarose-based biomaterials for tissue engineering, Carbohydr. Polym. 187 (2018) 66–84. https://doi.org/10.1016/j.carbpol.2018.01.060.

[38] C.T. Buckley, S.D. Thorpe, F.J. O'Brien, A.J. Robinson, D.J. Kelly, The effect of concentration, thermal history and cell seeding density on the initial mechanical properties of agarose hydrogels, J. Mech. Behav. Biomed. Mater. 2 (2009) 512–521. https://doi.org/10.1016/j.jmbbm.2008.12.007.

[39] K. Nijenhuis, Thermoreversible Networks - Viscoelastic properties and structure of gels, Springer Berlin, Heidelberg, 1997.

[40] C. Kim, D. Jeong, S. Kim, Y. Kim, S. Jung, Cyclodextrin functionalized agarose gel with low gelling temperature for controlled drug delivery systems, Carbohydr. Polym. 222 (2019) 115011. https://doi.org/10.1016/j.carbpol.2019.115011.

[41] C. Rochas, M. Lahaye, Average molecular weight and molecular weight distribution of agarose and agarose-type polysaccharides, Carbohydr. Polym. 10 (1989) 289-298.

[42] V. Normand, D.L. Lootens, E. Amici, K.P. Plucknett, P. Aymard, New insight into agarose gel mechanical properties, Biomacromolecules 1 (2000) 730–738. https://doi.org/10.1021/bm005583j.

[43] T. Singh, R. Meena, A. Kumar, Effect of sodium sulfate on the gelling behavior of agarose and water structure inside the gel networks, J. Phys. Chem. B 113 (2009) 2519–2525. https://doi.org/10.1021/jp809294p.

[44] D.C.D. Roux, F. Caton, I. Jeacomine, G. Maîtrejean, M. Rinaudo, Reversibility in the physical properties of agarose gels following an exchange in solvent and non-solvent, polymers, Polymers 16 (2024) 811. https://doi.org/10.3390/polym16060811.

[45] S. Arnott, A. Fulmer, W.E. Scott, I.C.M. Dea, R. Moorhouse, D.A. Rees, The agarose double helix and its function in agarose gel structure, J. Mol. Biol. 90 (1974) 269-272.

[46] M. Kouwijzer, S. Pérez, Molecular modeling of agarose helices, leading to the prediction of crystalline allomorphs, Biopolymers 46 (1998) 11-29.

[47] K. Alam, A. Hasan, M. Iqbal, J. Umer, S. Piya, Experimental study on the mechanical properties of biological hydrogels of different concentrations, Technol. Health Care 28 (2020) 685–695. https://doi.org/10.3233/THC-191984.

[48] Y. Mori, S. Kanazawa, M. Watanabe, H. Suenaga, K. Okubo, S. Nagata, Y. Fujihara, T. Takato, K. Hoshi, Usefulness of agarose mold as a storage container for three-dimensional tissue-engineered cartilage, Mater. Sci. Appl. 4 (2013) 73–78. https://doi.org/10.4236/msa.2013.48a010.

[49] Z. Guo, K. Hu, J. Sun, T. Zhang, Q. Zhang, L. Song, X. Zhang, N. Gu, Fabrication of hydrogel with cell adhesive micropatterns for mimicking the oriented tumor-associated extracellular matrix, ACS Appl. Mater. Interfaces 6 (2014) 10963–10968. https://doi.org/10.1021/am5023946.

[50] L.M. Barrangou, C.R. Daubert, E.A. Foegeding, Textural properties of agarose gels. I. Rheological and fracture properties, in: Food Hydrocoll, Elsevier, 2006: pp. 184–195. https://doi.org/10.1016/j.foodhyd.2005.02.019.

[51] T.A. Nguyen-Le, X. Zhao, M. Bachmann, P. Ruelens, J.A.G.M. de Visser, L. Baraban, High-throughput gel microbeads as incubators for bacterial competition study, Micromachines 14 (2023) 645. https://doi.org/10.3390/mi14030645.

[52] B.J. Staudinger, J.F. Muller, S. Halldórsson, B. Boles, A. Angermeyer, D. Nguyen, H. Rosen, Ó. Baldursson, M. Gottfreosson, G.H. Guomundsson, P.K. Singh, Conditions associated with the cystic fibrosis defect promote chronic Pseudomonas aeruginosa infection, Am. J. Respir. Crit. Care Med. 189 (2014) 812–824. https://doi.org/10.1164/rccm.201312-2142OC.

[53] J. Narayanan, J.-Y. Xiong, X.-Y. Liu, Determination of agarose gel pore size: Absorbance measurements vis a vis other techniques, Phys.: Conf. Ser. 28 (2006) 83-86. https://iopscience.iop.org/article/10.1088/1742-6596/28/1/017

[54] I. Jayawardena, P. Turunen, B. Cambraia Garms, A. Rowan, S. Corrie, L. Grøndahl, Evaluation of techniques used for visualisation of hydrogel morphology and determination of pore size distributions, Mater. Adv. 4 (2023) 669-682. https://doi.org/10.1039/D2MA00932C.

[55] J.J. Roberts, A. Earnshaw, V.L. Ferguson, S.J. Bryant, Comparative study of the viscoelastic mechanical behavior of agarose and poly(ethylene glycol) hydrogels, J.

759 Biomed. Mater. Res. B Appl Biomater. 99 (2011) 158–169.
760 https://doi.org/10.1002/jbm.b.31883.
761 [56] M. Sreepadmanabh, M. Ganesh, P. Sanjenbam, C. Kurzthaler, D. Agashe, T.
762 Bhattacharjee, Cell shape affects bacterial colony growth under physical confinement,
763 Nat. Commun. 15 (2024) 9561. https://doi.org/10.1038/s41467-024-53989-6.
764 [57] M.H. Zwietering, I. Jongenburger, F.M. Rombouts, K. van't Riet, Modeling of the
765 bacterial growth curve, Appl. Environ. Microbiol. 56 (1990) 1875-1881. https://doi:
766 10.1128/aem.56.6.1875-1881.1990
767 [58] C. Saint Martin, M. Darsonval, M. Grégoire, N. Caccia, L. Midoux, S. Berland, S. Leroy,
768 F. Dubois-Brissonnet, M. Desvaux, R. Briandet, Spatial organisation of Listeria
769 monocytogenes and Escherichia coli O157:H7 cultivated in gel matrices, Food
770 Microbiol. 103 (2022) 103965. https://doi.org/10.1016/j.fm.2021.103965
771 [59] T.R. De Kievit, B.H. Iglewski, Bacterial Quorum Sensing in pathogenic relationships,
772 Infect. Immun. 68 (2000) 4839-4849. https://doi.org/10.1128/iai.68.9.4839-4849.2000.
773 [60] S. Jeanson, J. Chadoeuf, M.N. Madec, S. Aly, J. Floury, T.F. Brocklehurst, S. Lortal,
774 Spatial distribution of bacterial colonies in a model cheese, Appl. Environ. Microbiol.
775 77 (2011) 1493–1500. https://doi.org/10.1128/AEM.02233-10.
776 [61] M. Lichtenberg, L. Kvich, S.L.B. Larsen, T.H. Jakobsen, T. Bjarnsholt, Inoculum
777 concentration influences Pseudomonas aeruginosa phenotype and biofilm architecture,
778 Microbiol. Spectr. 10 (2022). https://doi.org/10.1128/spectrum.03131-22.
779 [62] N. Kabanova, I. Stulova, R. Vilu, Microcalorimetric study of the growth of bacterial
780 colonies of Lactococcus lactis IL1403 in agar gels, Food Microbiol. 29 (2012) 67–79.
781 https://doi.org/10.1016/j.fm.2011.08.018.

[63] S. Jeanson, J. Floury, V. Gagnaire, S. Lortal, A. Thierry, Bacterial colonies in solid media and foods: A review on their growth and interactions with the micro-environment, Front. Microbiol. 6 (2015). https://doi.org/10.3389/fmicb.2015.01284.

[64] V.S. Tadimarri, M. Blanch-Asensio, K. Deshpande, J. Baumann, C. Baumann, R. Müller, S. Trujillo, S. Sankaran, PEARL: Protein eluting alginate with recombinant Lactobacilli, Small (2025) 2408316. https://doi.org/10.1002/smll.202408316.

[65] P.M. Fitch, A. Roghanian, S.E.M. Howie, J.-M. Sallenave, Human neutrophil elastase inhibitors in innate and adaptive immunity, Biochem. Soc. Trans. 34 (2006) 279-282. https://doi.org/10.1042/BST0340279.

[66] R. Decker, C. Burdelski, M. Zobiak, H. Büttner, G. Franke, M. Christner, K. Saß, B. Zobiak, H.A. Henke, A.R. Horswill, M. Bischoff, S. Bur, T. Hartmann, C.R. Schaeffer, P.D. Fey, H. Rohde, An 18 kDa scaffold protein is critical for staphylococcus epidermidis biofilm formation, PLoS Pathog. 11 (2015) e1004735. https://doi.org/10.1371/journal.ppat.1004735.

[67] M. Blanch-Asensio, S. Dey, S. Sankaran, In vitro assembly of plasmid DNA for direct cloning in Lactiplantibacillus plantarum WCSF1, PLoS One 18 (2023) e0281625. https://doi.org/10.1371/journal.pone.0281625.

[68] P. Thomas, A.C. Sekhar, R. Upreti, M.M. Mujawar, S.S. Pasha, Optimization of single plate-serial dilution spotting (SP-SDS) with sample anchoring as an assured method for bacterial and yeast cfu enumeration and single colony isolation from diverse samples, Biotechnol. Rep. 8 (2015) 45–55. https://doi.org/10.1016/j.btre.2015.08.003.